ELSEVIER

Soil Dynamics and Earthquake Engineering 21 (2001) 671–687

SOIL DYNAMICS AND EARTHQUAKE ENGINEERING

www.elsevier.com/locate/soildyn

Stiff soil amplification effects in the 7 September 1999 Athens (Greece) earthquake

G.D. Bouckovalas*, G.P. Kouretzis

Geotechnical Division, Department of Civil Engineering, National Technical University of Athens, Patission 42, 10682 Athens, Greece

Accepted 13 July 2001

Abstract

The Athens, Greece, earthquake of 7 September 1999 provided a number of reliable strong motion recordings and well-defined patterns of damage at sites with known geological and geotechnical conditions. Joint evaluation of this evidence shows that the very stiff soils of the Athens basin, compared to the nearby outcropping soft rocks, have amplified the peak horizontal acceleration by an average of 40% or more and have shifted elastic response spectra to higher periods. US and the European seismic code provisions (NEHRP-97 and EC-8), place stiff soils and soft rocks at the same site category and consequently fail to predict these adverse effects. A larger number of site categories and new site coefficients that depend on the seismic excitation frequency appear necessary in order to overcome this deficit of the codes.

Keywords: Athens earthquake; Site characterization; Seismic codes; Soil amplification

1. Introduction

On 7 September 1999 (11:56:50.5 GMT) a violent earthquake of $Ms = 5.9$ struck the western bounds of the greater metropolitan area of Athens, at 18 km distance from the historical center. According to official accounts, it was one of the most damaging events in the modern history of Greece, and certainly the most damaging for the city of Athens. About 100 buildings collapsed, raising the number of casualties to 143. Reported injuries were as high as 2000 while more than 100,000 people were rendered homeless. Some historical monuments suffered significant damage, like the Byzantine monastery of Dafni and the 5th century BC castle of Fili, while ancient monuments have resisted the earthquake impressively well.

Most of the damage concerned residential or factory buildings and occurred within 15 km of the epicenter and 7 km from the fault rupture, which is identified for simplicity as the trace of Fili fault in Fig. 1. The damage to lifelines was insignificant while no major ground failures (liquefaction, slope failures, etc.) were triggered by the earthquake. The maximum intensity in Modified Mercali scale reached IX at the epicentral area and exceeded VI in the greater part of Athens. The distribution of damage within the affected zone was irregular, creating speculation for rupture directivity and local site amplification phenomena.

Following a brief seismological review, this paper presents results from a site-specific analysis of main-shock strong motion recordings and the on-going correlation of damages to local soil conditions. Special emphasis is given to the stiff soil amplification phenomena that emerged during the earthquake. The reason is that such phenomena are rarely observed in nature since, theoretically at least, they are associated with comparatively high frequency excitations. Furthermore, they are overlooked by current seismic codes which do not differentiate stiff soils from soft or even firm rocks. To estimate the potential deficit in seismic design actions due to this reason, field data from this earthquake are compared to the provisions of two modern seismic codes, [1] and the revised [2], which propose recently refined site classification schemes.

For more general information on the Athens earthquake of 7 September 1999, the reader is referred to the list of additional bibliography following the references of the article.

2. Seismological aspects and strong motion recordings

Table 1 summarizes the focal parameters of the main-shock, according to a number of independent fault plane solutions based either on teleseismic or near-field station

* Corresponding author. Tel.: +30-1-772-3780; fax: +30-1-772-3428.
E-mail address: g.bouck@civil.ntua.gr (G.D. Bouckovalas).

0267-7261/01/$ - see front matter
PII: S0267-7261(01)00045-8

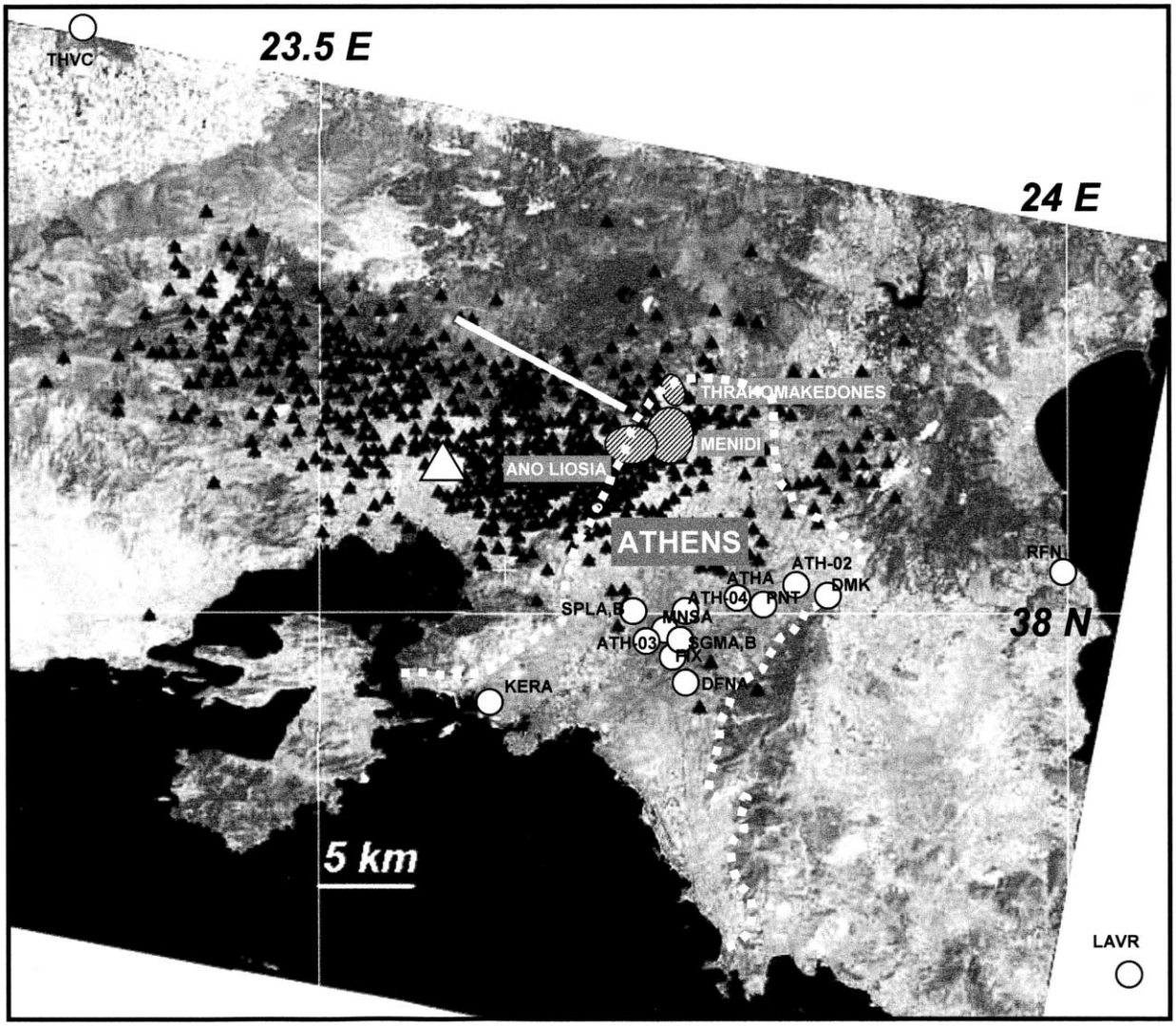

Fig. 1. Map of the epicentral area of Athens 7 September 1999 earthquake. Black hollow triangles indicate aftershock epicenters; the white triangle corresponds to the epicenter of the main shock, while white spots stand for strong motion recording sites. The white continuous line represents the simplified trace of Fili fault.

recordings. The prevailing view regarding the location of the mainshock epicenter is shown in the map of Fig. 1, together with the distribution of the aftershock epicenters recorded during the period from 8 September to 29 October 1999 by the [10]. In addition, Fig. 2 shows the 3-D perspective of the mainshock and aftershock epicenters, the fault plane and the direction of rupture ([11]).

In general, there is consensus that the earthquake was due to a normal fault rupture, striking N 110–123° and dipping 47–56° SW. Most likely, the rupture originated at a depth of

Table 1
Focal parameters of the main shock reported by various agencies

Agency	Moment (Nm)	Depth (km)	Strike (deg)	Dip (deg)	Lat. (deg N)	Long (deg E)
[3]	7.8e17	9	123	55	38.13	23.55
[4]	1.2e18	15	114	47	38.02	23.71
[5]	7.6e17	11 ÷ 18	119	56	38.04	23.61
[6]	5.66e17	10	117	52	–	–
[7]	–	16	113	56	38.10	23.58
[8]	–	8	110	55	–	–
[9]	–	10	117	52	–	–

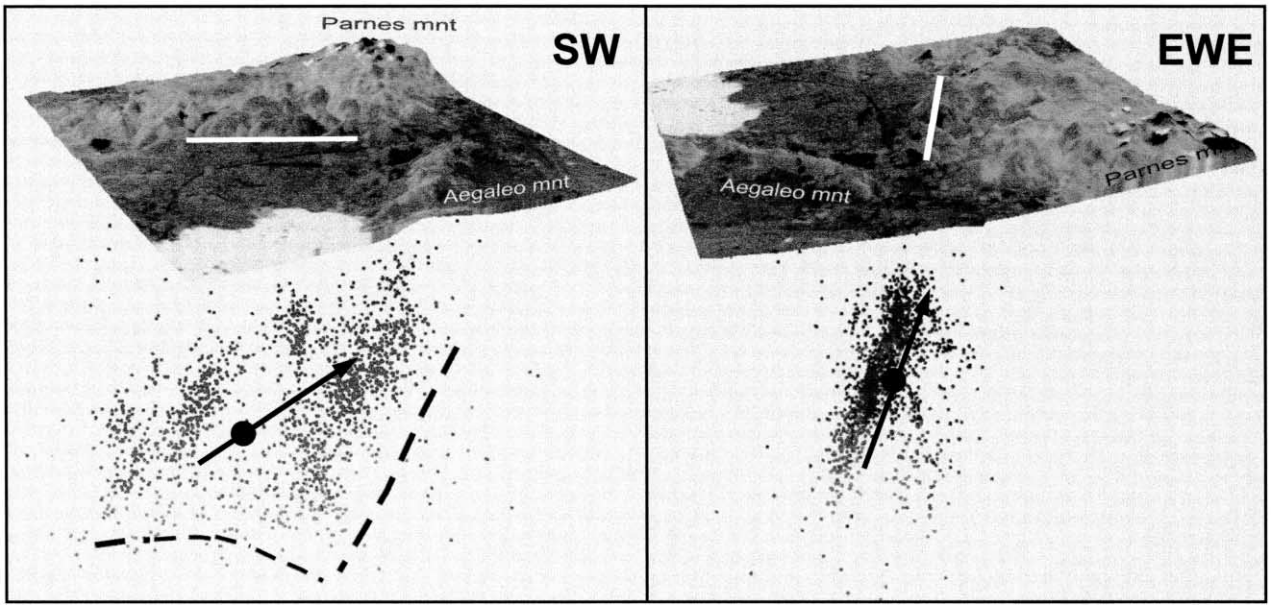

Fig. 2. Isometric views from south-west and east-south-east of the main shock and aftershock epicenters, denoted by a large circle and small dots respectively. The black dashed line bounds the fault plane while the arrow shows the direction of rupture. The continuous white line represents the simplified trace on the ground surface of Fili fault.

8–18 km and propagated from southwest to northeast and upwards ([7,12,13]) creating strong directivity effects on seismic ground motions. Apart from fault plane solutions, this view is confirmed by the analysis of regional broadband seismograms ([12]), which revealed shorter apparent source duration to the NNE of the epicenter (4–5 s) and a longer one to the SSW (7–8 s). The approximate slip length at rupture is estimated to 300 mm, based on ERS2 satellite radar interferrometry ([14]).

Note that the fault plane geometry is similar to the geometry of a number of regional tectonic faults. This observation, combined with geologic and seismotectonic field investigations mainly reported by ([15,16]) support the hypothesis that the earthquake rupture occurred on a pre-existing fault plane, most probably the plane of Fili fault (Fig. 1), and has propagated all the way up to the ground surface. However, this view is considered with skepticism for two main reasons. The first is that neither the Fili fault nor any other of the regional tectonic faults was considered active prior to the earthquake. In fact, the historical seismicity record of Athens appears to have been free of destructive earthquakes ([17]) and the entire area was assigned the second lowest seismicity level by the national seismic code. The second reason is that the reported evidence of ground rupture (soil cracks, rock falls etc.) was limited and leaves doubts as to whether the rupture has actually propagated to the ground surface ([18,19]). This argument is also supported by [8] based on the distribution with depth of recorded aftershock epicenters (e.g. Fig. 2). In conclusion, the view prevailing today is that the earthquake was caused by a blind fault that intersects the ground surface at a trace similar to that of Fili fault.

The strong ground motion from the main shock of the Athens Earthquake has been recorded by 18 accelerographs, located as shown in the map of Fig. 1: fourteen within the central area of Athens and four at the center of nearby towns of Rafina, Lavrio, Aliveri and Thiva. Table 2 includes practical information regarding the recordings, i.e. the distance from rupture, the peak acceleration and velocity, the significant period range, the local geology and a description of the recording station. To outline the basic features of recorded seismic ground motion, Fig. 3 shows the acceleration time histories and the elastic response spectra of one typical recording (SPLB) obtained at the surface of stiff alluvial deposits, under practically free field conditions. Observe the short apparent duration and the relatively high frequency (low period) of the motion. According to [9], the first of these features supports an asperity-like model for the source, characterized by a very short rise time (0.1–0.2 s) and a nearly complete stress release, that led to the relatively high recorded accelerations. Furthermore, the second feature is interpreted as a Doppler effect created due to rupture directivity.

3. Site characterization of recordings

It is fortunate that most of the recording sites lay in the vicinity of major public works, such as surface or underground stations of the Athens subway system (METRO). Thus, it has been possible to collect data from pre-existing geotechnical investigations and define the local geological and geotechnical conditions at the recording sites. A complementary assessment of site conditions was obtained directly from the available seismic recordings, based on the

Table 2
Documentation of strong motion recordings

Recording	Component	Distance from rupture (km)	a_{max} (g)	v_{max} (m/s)	Significant period range	Geological conditions	Location of instrument
ATHA (Neo Psihiko)	Long	12	0.084	0.053	0.18–0.27	Tertiary deposits	Three-storey RC—private build.
	Trans		0.101	0.074	0.13–0.17		
	Vert		0.114	0.034	0.05–0.07		
MNSA (monastiraki)	Long	13	0.229	0.149	0.12–0.22	Manmade deposits/weathered schist/phyllite	Free field—Metro station
	Trans		0.512	0.149	0.13–0.19		
	Vert		0.162	0.035	0.04–0.07		
SPLB (Sepolia)	Long	9	0.324	0.214	0.20–0.34	Manmade deposits/alluvium/weathered schist	Three-storey steel build.—Metro garage
	Trans		0.312	0.189	0.15–0.33		
	Vert		0.192	0.074	0.08–0.14		
DMK (Ag. Paraskevi)	Long	16	0.046	0.025	0.08–0.13	Weathered limestone	Small RC house—Democritus Institute
	Trans		0.076	0.025	0.09–0.13		
	Vert		0.038	0.030	0.10–0.14		
ATH-02 (Chalandri)	Long	12	0.110	0.051	0.11–0.20	Alluvium/weathered schist	Two-storey RC build.—town hall
	Trans		0.159	0.069	0.08–0.25		
	Vert		0.092	0.034	0.08–0.11		
ATH-03 (Kallithea)	Long	13	0.264	0.161	0.09–0.13	Alluvium/weathered schist	One-storey RC build.—(K.E.D.E.)
	Trans		0.303	0.147	0.19–0.26		
	Vert		0.157	0.070	0.04–0.07		
ATH-04 (Kipseli)	Long	12	0.121	0.089	0.09–0.11	Weathered schist	Three-storey RC build.—(G.Y.S.)
	Trans		0.110	0.085	0.11–0.30		
	Vert		0.053	0.034	0.07–0.12		
KERA (Keratsini)	Long	14	0.223	0.100	0.17–0.40	Tertiary deposits	Electric Power Plant (D.E.H.)
	Trans		0.186	0.073	0.20–0.27		
	Vert		0.155	0.042	0.06–0.13		
SPLA (Sepolia)	Long	9	0.255	0.179	0.09–0.13	Alluvium/weathered schist	−2 level (−13 m)—Metro station
	Trans		0.221	0.128	0.19–0.52		
	Vert		0.082	0.059	0.05–0.07		
SGMA (Syntagma)	Long	13	0.149	0.127	0.10–0.18	Weathered schist	−1 level (−7 m)—Metro station
	Trans		0.239	0.134	0.13–0.17		
	Vert		0.054	0.030	0.11–0.21		
SGMB (Syntagma)	Long	13	0.111	0.099	0.19–0.29	Weathered schist	−3 level (−26 m)—Metro station
	Trans		0.087	0.108	0.23–0.59		
	Vert		0.089	0.036	0.13–0.16		
DFNA (Dafni)	Long	16	0.045	0.044	0.12–0.23	Alluvium/weathered schist	−2 level (−14 m)—Metro station
	Trans		0.080	0.077	0.16–0.25		
	Vert		0.041	0.028	0.11–0.18		
PNT (Papagou)	Long	13	0.088	0.076	0.16–0.25	Tertiary deposits	−2 level (−15 m)—Metro station
	Trans		0.079	0.051	0.15–0.27		
	Vert		0.055	0.038	0.08–0.11		

Table 2 (*continued*)

Recording	Component	Distance from rupture (km)	a_{max} (g)	v_{max} (m/s)	Significant period range	Geological conditions	Location of instrument
FIX (Sygrou-Fix)	Long	15	0.086	0.079	0.17–0.22	Alluvium/weathered schist	−2 level (−15 m)—Metro station
	Trans		0.124	0.110	0.16–0.29		
	Vert		0.046	0.035	0.08–0.14		
RFN (Rafina)	Long	27	0.081	0.035	0.09–0.12	Tertiary deposits/limestone	Small wooden house—private building
	Trans		0.100	0.053	0.09–0.15		
	Vert		0.030	0.029	0.04–0.11		
ALIV (Aliveri)	Long	47	0.020	0.009	0.20–0.23	Neogene marls	Electric Power Plant (D.E.H.)
	Trans		0.017	0.009	0.11–0.23		
	Vert		0.010	0.005	0.10–0.14		
LAVR (Lavrio)	Long	52	0.042	0.020	0.06–0.11	Weathered schist/limestone	Electric Power Plant (D.E.H.)
	Trans		0.053	0.018	0.22–0.30		
	Vert		0.048	0.018	0.22–0.31		
THVC (Thiva)	Long	30	0.058	0.036	0.27–0.42	Conglomerate	Three-storey RC—town hall
	Trans		0.056	0.026	0.09–0.11		
	Vert		0.044	0.019	0.17–0.23		

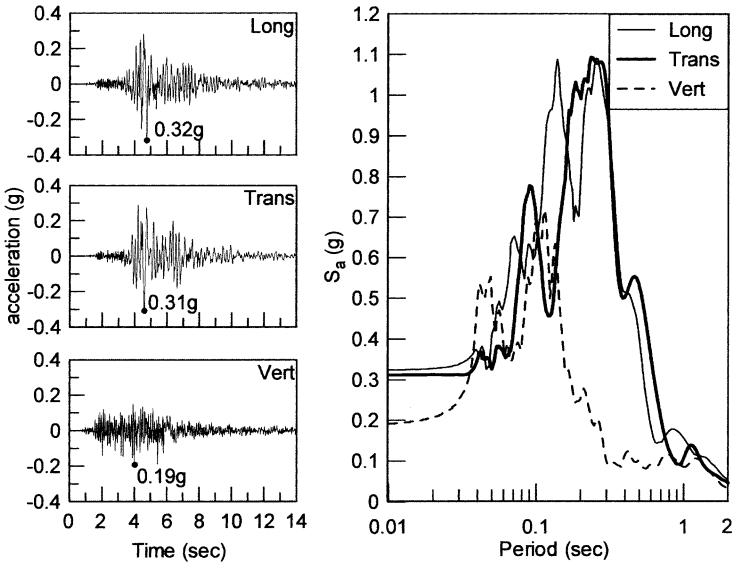

Fig. 3. Acceleration time histories and elastic response spectra from a typical surface recording of the main shock, at 9 km distance from fault rupture.

horizontal-to-vertical spectral ratio (HVSR) method. The HVSR has been initially applied for quick, in situ estimates of the fundamental site period from the Fourier spectra of microtremors ([20]). Later, its use has been also extended to strong seismic motion recordings, with encouraging results (e.g. [21–26]).

In the present study, the HVSR is applied only to strong motion recordings obtained on the ground surface, using the normalized elastic response spectra (for 5% damping) instead of the Fourier spectra mostly used in the literature. The reason for this modification, referred briefly here after as Normalized Horizontal-to-Vertical Spectral Ratio or NHVSR, is demonstrated in Fig. 4 which compares NHVSR to HVSR for two typical recordings: THVC on neogene, soft rock formations and SPLB on dense alluvial deposits. Observe that the two spectral ratios are grossly similar, but HVSR is very sensitive to the amount of smoothing applied and cannot be interpreted as clearly as the NHVSR. Focusing on the NHVSR, it is further observed that not only the fundamental site period but also the peak of the spectral ratio increases, as the soil column becomes more flexible. Namely, the peak value increases from 2.13 to 4.85 as the fundamental period increases from 0.10 to 0.30 s. Note that the use of elastic response spectra instead of Fourier spectra, for quantitative estimates of frequency related soil parameters from seismic motions, is presently gaining ground among engineers as well as seismologists (e.g. [27–29]).

Table 3 summarizes the site period derived with the NHVSR method (T_{NHVSR}) and the peak value of NHVSR

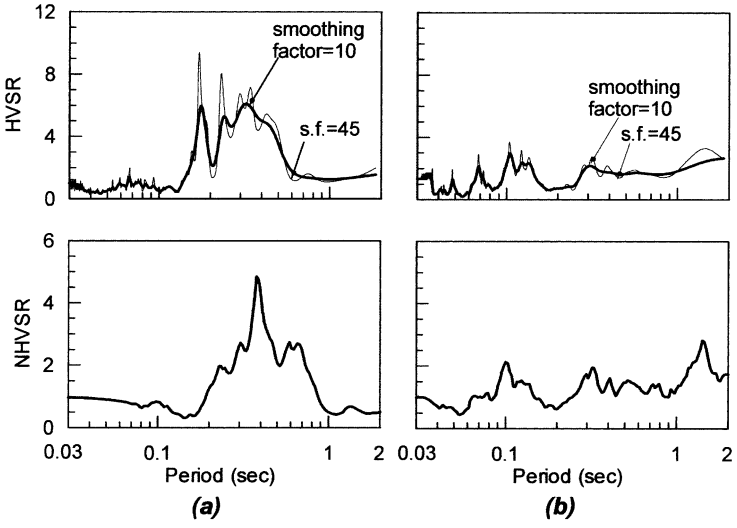

Fig. 4. Application of the horizontal-to-vertical spectral ratio (HVSR) and normalized horizontal-to-vertical spectral ratio (NHVSR) methods for two recordings obtained on the surface of (a) stiff soil and (b) soft rock geological formations.

Table 3
Site characterization parameters deduced from seismological and geotechnical data

Recording[a]	Component	T_{NHVSR}	A_{NHVSR}	$V_{s,30b}$[b] (m/s)	Soil category
ATHA	Long	0.32	3.74	367	Stiff Soil
	Trans	0.31	0.48		
MNSA	Long	0.40	5.21	403	Stiff Soil
	Trans	0.20	3.81		
SPLB	Long	0.30	4.46	410	Stiff Soil
	Trans	0.30	4.85		
DMK	Long	0.11	1.33	> 550	(Soft) Rock
	Trans	0.15	1.47		
ATH-02	Long	0.30	3.77	428	Stiff Soil
	Trans	0.14	2.36		
ATH-03	Long	0.24	2.80	472	Stiff Soil
	Trans	0.22	3.16		
ATH-04	Long	0.48	2.71	399	Stiff Soil
	Trans	0.48	2.31		
KERA	Long	0.31	3.25	404	Stiff Soil
	Trans	0.32	3.32		
RFN	Long	0.12	2.15	> 550	Soft Rock
	Trans	0.14	1.67		
ALIV	Long	0.22	1.56	> 550	Soft Rock
	Trans	0.17	2.36		
LAVR	Long	0.09	2.50	> 550	Soft Rock
	Trans	0.08	2.31		
THVC	Long	0.31	2.75	559	Soft Rock
	Trans	0.10	2.13		

[a] Underground recordings (SPLA, SGMA, SGMB, DFNA, PNT, FIX) are not classified.
[b] From Eq. (1).

(A_{NHVSR}) for the two horizontal components (LONG and TRANS) of the seismic ground motion at the recording sites. In addition, Fig. 5 correlates A_{NHVSR} to the fundamental site period T_{NHVSR} obtained from ground surface recordings. The correlation is reasonably well established, exhibiting a coefficient of determination $r^2 = 0.91$. Furthermore, it shows that A_{NHVSR} is more sensitive to soil conditions and T_{NHVSR}. More specifically, computing the range of variation for these two variables as the (standard deviation/average) ratio yields 0.63 for A_{NHVSR} and 0.45 for T_{NHVSR}. It is noted that reported statistics for A_{NHVSR} were actually deduced from an analysis of $(A_{NHVSR} - 1)$ values, taking into account that, by definition, $A_{NHVSR} \approx 1$ at outcropping bedrock ($T_{NHVSR} \approx 0.0$)

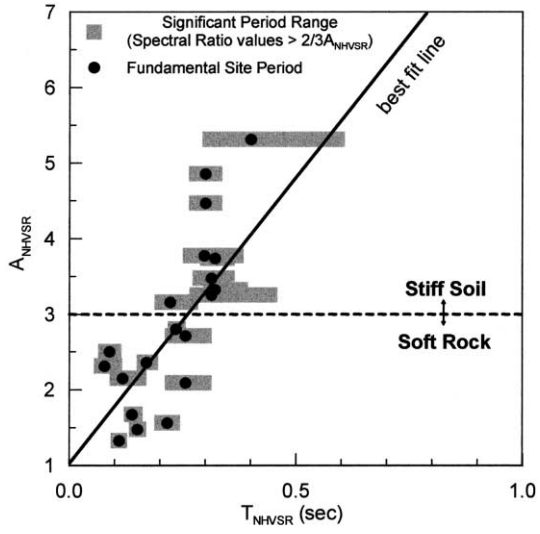

Fig. 5. Correlation of site periods deduced from the NHVSR method (T_{NHVSR}) with the corresponding peak value of the normalized elastic response spectra ratio (A_{NHVSR}).

Based on the local geological-geotechnical conditions, but also on the results from the NHVSR method described above, recording sites at ground surface level were classified in two groups.

Group I: *Soft rock sites* consist of weathered schist and limestone (DMK and LAVR sites), cohesive talus cones and medium to well-cemented conglomerates (THVC site) or neogene marls (RFN and ALIV sites). For all sites A_{NHVSR} is less than 3, T_{NHVSR} varies between 0.07 and 0.26 s, while the average shear wave velocity over the top 30 m ($V_{S,30}$) is greater than about 500 m/s.

Group II: *Stiff soil sites* consist of moderately thick weathering products of the geological bedrock (ATHA, ATH-04 and KERA site), alluvium deposits of medium to high density (ATH-02, ATH-03 and SPLB sites) or recent manmade deposits (MNSA site). In this category, A_{NHVSR} is greater than 3, T_{NHVSR} varies from 0.22 to 0.50 s and $V_{S,30}$ ranges between 367 and 472 m/s.

The values of average shear wave velocity $V_{S,30}$ reported for the two groups of sites have been estimated indirectly, from standard penetration test results, as it is explained in the following section.

According to conventional engineering practice, distinction between the above categories would not be as significant as their geological origin may imply. That is, seismic code definitions would not distinguish between the different sites and categorize them in the same group. For example, all recording sites belong to Site Class C of NEHRP-97 (soft rock/very stiff soil with $V_{S,30} = 360 \div 760$ m/s) and to Subsoil Class B of the revised EC8 (very dense/stiff soil with $V_{S,30} = 360 \div 800$ m/s).

4. Analysis of strong motion recordings

From Fig. 1, it may be observed that all recordings sites, except from THVC in the town of Thiva, lay to the east of the rupture zone and on the hanging wall side of the fault. Furthermore, they correspond to a wide range of fault distances ($9 \div 52$ km) and consequently they may provide evidence for the attenuation of seismic motion with distance from the fault rupture. To increase the number of data points used to define the attenuation of seismic ground motion, actual recordings of the free ground motion were supplemented with site compatible analytical predictions,

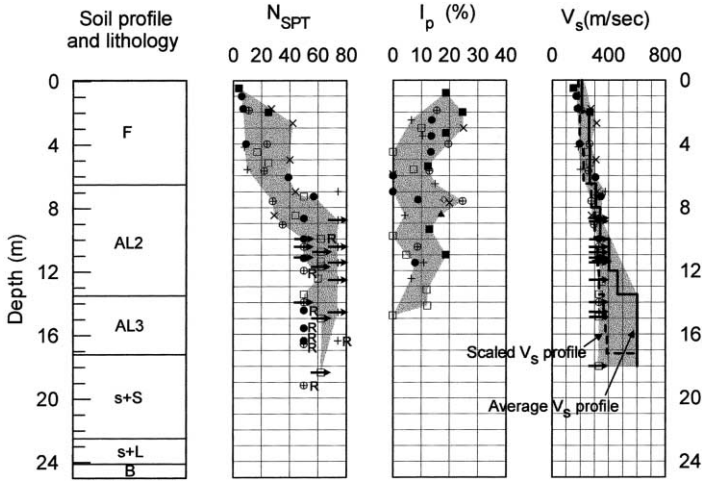

Fig. 6. Geotechnical profile for the SPLA and SPLB sites at Sepolia subway station (symbols and lithology notation are explained in Appendix A).

based on the 1-D equivalent linear method ([30]). The site response analyses were primarily aimed to transfer seismic motions recorded on the free surface of soil sites to the surface of the outcropping bedrock, i.e. a hypothetical bedrock site at the location of the recording. The average shear wave velocity of bedrock was taken as 550 m/s, as for the Soft Rock formations of the first group of recording sites.

Definition of the soil properties required for the seismic response analyses faced two objective difficulties. The first is that geotechnical investigations were generally performed in the wider rather than the close vicinity of the recording sites, some times at a distance of 100 ÷ 200 m. As a result, the soil properties at each depth were defined as a possible range instead of a single value. The second difficulty is that the investigations did not include the special tests required to measure directly the dynamic soil properties. Hence, the shear wave velocity of the soil layers V_S was estimated indirectly from Standard Penetration Test measurements N_{SPT}, as ([31]):

$$V_S \text{ (m/s)} = 97.0\, N_{SPT}^{0.314} \quad (1)$$

Furthermore, the non-linear hysteretic response of soil to earthquake-induced dynamic shear deformations has been specified in connection to the plasticity index I_P, according to the empirical relations of [32]. A typical soil profile constructed with this procedure is shown in Fig. 6. It is based on the geotechnical data collected for the wider area of Sepolia subway station, the location of two recording sites: SPLB on the free ground surface and SPLA within the underground subway station. Similar profiles could be constructed for all but three sites (LAVR, ALIV and RFN), as reported by [33].

Two analyses were performed for every recording site, one for each component of the seismic excitation, starting with the average soil properties denoted with bold line in the typical profile of Fig. 6. To obtain a gross feeling of the compatibility between analytical predictions and seismological methods for site characterization, Fig. 7 compares T_{NHVSR} to T_{1-D}. The data corresponding to the TRANS components of MNSA and ATH-02 records have been excluded from the comparison, as possibly affected by dynamic soil-structure interaction phenomena. Observe that the two independent site periods estimates correlate reasonably well, but T_{NHVSR} is

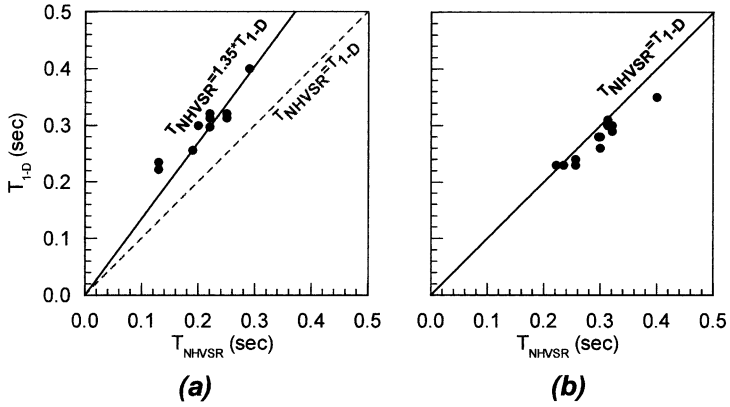

Fig. 7. Comparison between fundamental site periods obtained from the NHVSR method and site periods analytically computed for (a) average V_S profiles and (b) scaled V_S profiles.

Table 4
Results from seismic ground response analyses

Recording	Component	Depth (m)	T_s		a_{max} surface (g)	a_{max} outcropping bedrock (g)	
			Average[a]	Scaled[b]		Average[a]	Scaled[b]
ATHA	Long	0	0.25	0.31	0.083	0.046	0.044
	Trans				0.101	0.067	0.066
MNSA	Long	0	0.29	0.35	0.233	0.170	0.155
	Trans				0.511	0.407	–
SPLB	Long	0	0.20	0.28	0.239	0.143	0.150
	Trans				0.407	0.310	0.234
ATH-02	Long	0	0.22	0.28	0.110	0.081	0.075
	Trans				0.159	0.113	–
ATH-03	Long	0	0.13	0.23	0.265	0.234	0.209
	Trans				0.302	0.236	0.182
ATH-04	Long	0	0.19	0.24	0.121	0.089	0.089
	Trans				0.110	0.069	0.069
KERA	Long	0	0.22	0.30	0.223	0.172	0.159
	Trans				0.186	0.118	0.154

[a] Average soil properties.
[b] Scaled soil properties.

systematically higher than T_{1-D} by an average of 35% [Fig. 7(a)]. To improve agreement, the analyses were repeated using a more or less uniform scaling of the initial shear wave profile (dotted line in Fig. 6), without violating the range of data obtained from the geotechnical investigations. The average reduction in shear wave velocity required to close the gap between T_{1-D} and T_{NHVSR} [Fig. 7(b)] is merely 5–20% and has a relatively minor effect on predicted ground and spectral accelerations. Results from all seismic response analyses are listed in Table 4.

The attenuation of peak horizontal and peak vertical acceleration with distance from the fault rupture is shown in Fig. 8(a) and (b), respectively. In each figure, a distinction is made between the data points corresponding to the two site groups identified in the previous section. Furthermore, in Fig. 8(a), the bullets denote ground surface recordings while the triangles denote the site compatible analytical predictions. According to these data, local soil conditions appear insignificant for the vertical peak ground accelerations but grossly differentiate the peak horizontal acceleration values for the Soft Rock and the Stiff Soil formations.

To obtain a quantitative estimate of this effect, continuous curves are drawn to depict the average trend of the data points, using as reference the attenuation relations proposed by [34] for similar seismotectonic and geological conditions. Thus, for distances between 9 and 15 km from the rupture, where the majority of soil recordings belong, the average attenuation curves yield an approximate 40% amplification at Stiff Soil sites relative to Soft Rock sites.

The effect of local soil conditions on the frequency content of ground motion is demonstrated in Figs. 9 and 10 through comparison of the normalized elastic response spectra from all available ground surface recordings. Normalization of the elastic spectral accelerations, against the peak horizontal ground acceleration, aims to minimize the effect of fault rupture distance on the data. More specifically, Fig. 9(a) and (b) summarize the spectra (range and average) for Soft Rock sites and for Stiff Soil sites

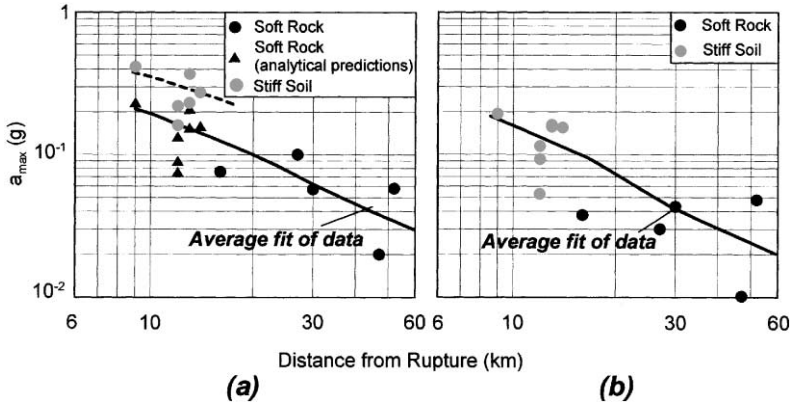

Fig. 8. Attenuation of peak horizontal (a) and peak vertical (b) acceleration with distance from fault rupture.

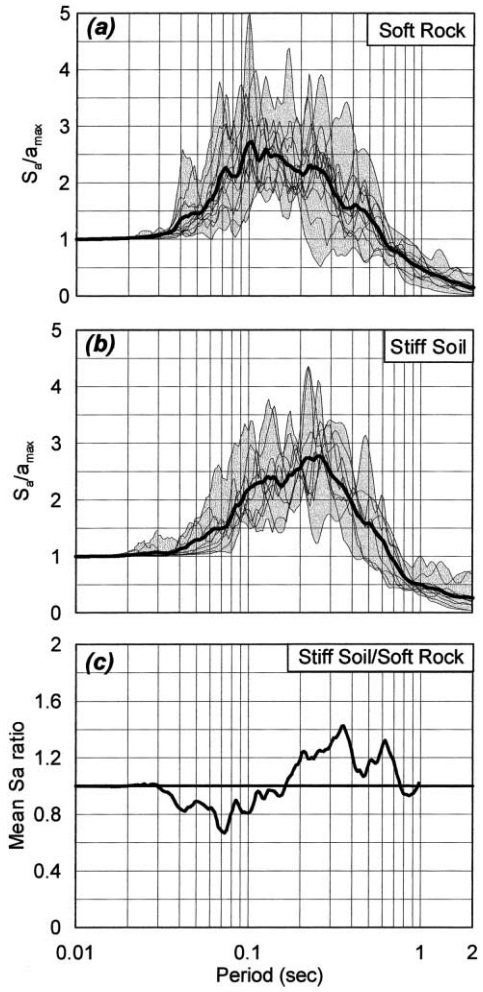

Fig. 9. (a) Normalized elastic response spectra (5% damping) for Soft Rock sites, (b) Normalized elastic response spectra (5% damping) for Stiff Soil sites and (c) Ratio of the average spectra for Stiff Soil over Soft Rock sites.

respectively, while Fig. 9(c) shows the ratio of the average spectrum for Stiff Soil sites over that for Soft Rock sites.

Observe that the peak of the average spectra for Soft Rock and Stiff Soil sites are approximately the same but there is a clear shift in the corresponding predominant periods, approximately from 0.10 s for the first group of sites to 0.25 s for the second. In addition, the ratio of the two spectra suggests that Stiff Soil sites amplify the higher period ($T = 0.17–1.00$ s) and de-amplify the lower period ($T = 0.03–0.17$) components of the seismic ground motion. In average terms, the Stiff Soil-to-Soft Rock spectral ratio varies between a maximum of 1.45 (amplification) and a minimum of 0.65 (de-amplification).

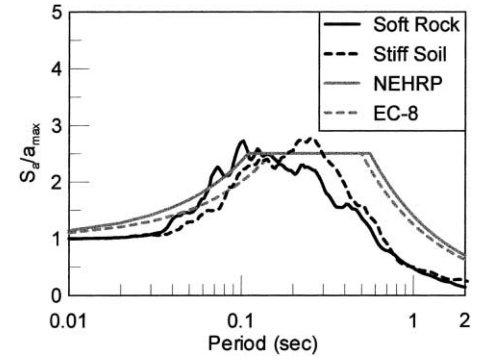

Fig. 10. Comparison of the average normalized spectra for Stiff Soil and Soft Rock sites with the normalized design spectra of NEHRP and EC-8 for similar earthquake characteristics.

Taking into account that the peak of the normalized horizontal to vertical spectral ratio (A_{NHVSR}) for Stiff Soil, that is also a measure of soil effects, is greater than 3.00 (Table 3), it is realized that the above differences are rather minor. In support of this evidence, the average normalized elastic response spectra for the two groups of recording sites fit reasonably well under the design spectra provided by seismic codes for relevant ground conditions. The comparison is shown in Fig. 10, where the average spectra of Fig. 9(a) and (b) are compared to typical design spectra for site class C of NEHRP-97 and subsoil class B of [2]. To simulate the characteristics of the Athens (7 September 1999) earthquake, the design spectra have been drawn for a peak ground acceleration of 0.30 g and $Ms > 5.5$.

5. Analysis of damage distribution

Additional evidence for stiff soil amplification of the seismic ground motion is deduced indirectly, from the analysis of damages reported in the meizoseismal area of the earthquake. The case study presented herein concerns the municipality of Ano Liosia, at 1–3 km distance from the rupture zone (Fig. 1), which was literally devastated during the earthquake. Among the 8220 buildings of the area, about 1085 (13%) collapsed or had to be demolished, while another 3030 (37%) required major repair. The map of Fig. 11 summarizes the damage statistics over the entire municipality with the aid of pie charts. The black, gray and white colors correspond to severe, moderate and light damages, according to the definitions of Table 5. It is evident that the distribution of damage is not uniform, with severe damages concentrated within the central-southern part of the municipality.

To assess the role of soil conditions in the irregular distribution of damages, a thorough geotechnical investigation was carried out, including downhole measurement of shear wave velocity V_S at 14 locations ([35]). For instance, Fig. 12 shows the correlation of building damages to local ground conditions along a north-to-south section passing through the center of the municipality. The top part of this figure includes the damage statistics in the form of bar charts while the lower part shows the associated geological and shear wave velocity (V_s) profiles.

It is observed that subsoil is dominated by loosely to well cemented conglomerates up to a minimum depth of about 25 m, and by stiff marls at greater depths. The average shear

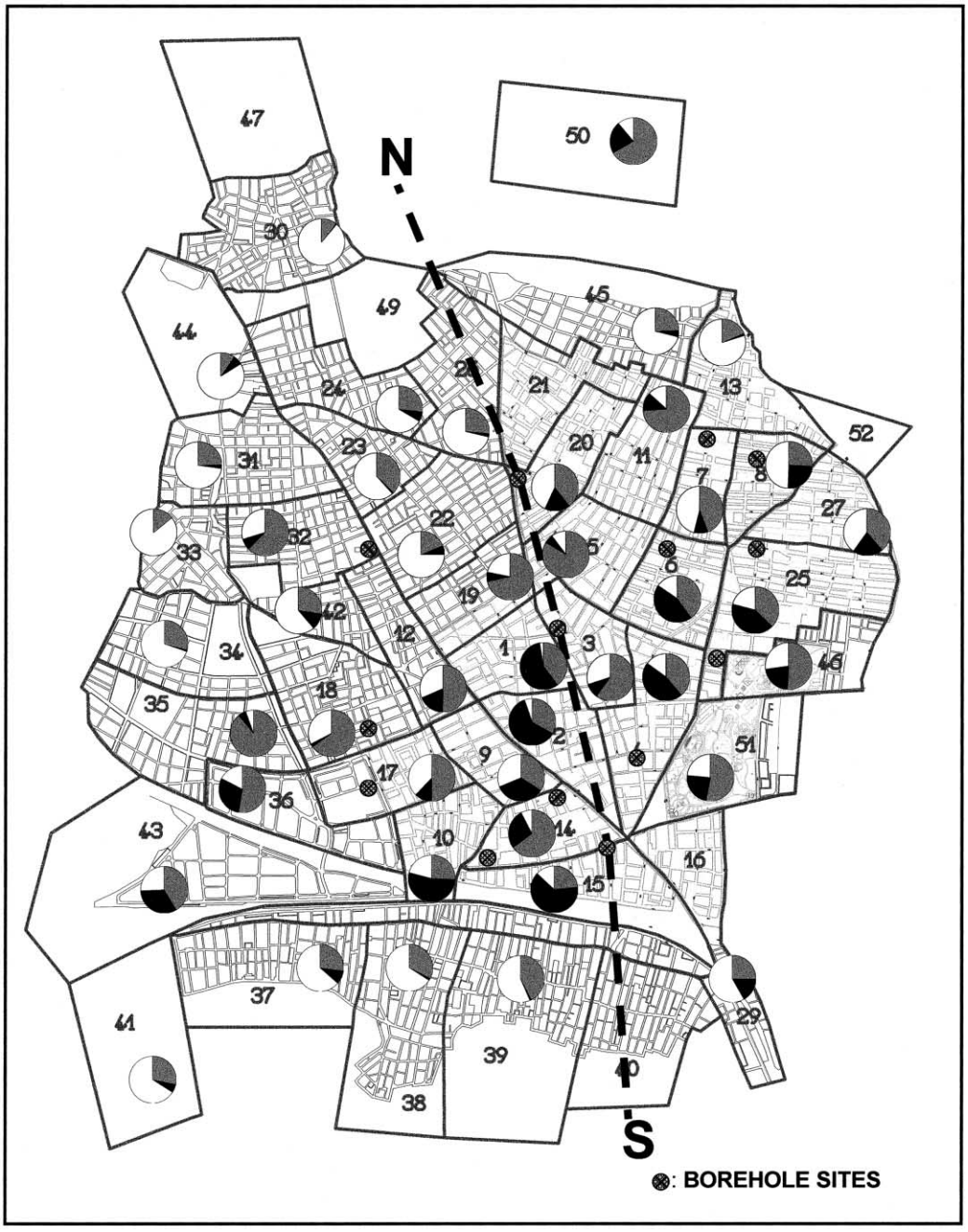

Fig. 11. Damage statistics over the entire Ano Liosia municipality, summarized with the aid of pie charts for 52 areas.

wave velocity at the top 30m of depth ($V_{s,30}$) ranges between 697 and 496 m/s, with a clear tendency to decrease gradually from north to south. According to the categorization adopted for the recorded sites, the northern part of the cross-section (boreholes CHT2 and DH8) belong to the group of Soft Rock sites while the central-southern part of the section (DH11, DH10, DH5) belong to the Stiff Soil group. On the contrary, these formations are considered more or less uniform in the premise of seismic codes (i.e. Site Class C of NEHRP-97 or Subsoil Class B of the revised EC-8).

The damage profile changes also along the cross-section: the percentage of buildings with severe damage increases from 3% in the north to 50–60% in the center-south, while the percentage of buildings with light damage decreases from 75% to 5–10%, respectively. The possible effect of structural factors on the aforementioned distribution of damages is investigated in Table 6, for two representative regions: the wider area of borehole CHT2 in the north and the wider area of boreholes DH11, DH10 and DH5 in the south, the former containing 155 buildings and the later 486 buildings. The statistics presented in this table concern the

Table 5
Description of building damage classification system

Light damage	No major damages; antiseismic capacity not reduced; the building is suitable for immediate use	• Light cracks on fill masonry walls and ceiling lime-cast • Trichoid, non-diagonal cracks on horizontal R/C structural elements
Moderate damage	Antiseismic capacity has been reduced; for safety reasons the building should not be used until the heave of jeopardy in facial or other non-bearing elements; possible need for extra support elements; possible need for dethronement of lime-cast until the final heave of jeopardy; the building is temporarily unsuitable for use (restricted entrance on own risk)	• Detachment of lime-cast flakes • Light damages/partial or complete sliding/falling of roof compartments • Damages or partial failure in chimneys, attics and parapets • Diagonal or other cracks on load-bearing masonry walls • Diagonal cracks or shattering of walls between doors/windows • Cracks in structural R/C elements (e.g. columns) • Damage/collapse/warping of the roof • Light, permanent deformation of structural elements
Severe damage	The building has suffered heavy damage; risk of collapse (not usable—entrance is strictly prohibited)	• Partial or total collapse of the building or of a single storey *For RC buildings:* • load-bearing elements suffer severe damages and permanent deformation • heavy damages in joints/junctures • major deformations of the building or of a single storey *For masonry buildings:* • significant rake • severe cracks • decay of wall mass

number of storeys, the type of the load-bearing structure and the year of construction in relation to the dates of major updates in the national seismic code provisions. It is clear that building properties are more or less uniform and that the significant bias in damages observed in Figs. 11 and 12 cannot be attributed to structural causes. In fact, the overall seismic resistance of buildings, projected from the type of the load-bearing structure, is enhanced in the southern area that includes relatively more R/C and less masonry buildings.

To verify the impact of soil conditions, the seismic ground response was estimated analytically for borehole sites CHT2 in the northern region of least damage, and DH5 in the severely damaged southern region. The analyses were performed with the equivalent linear, 1-D wave propagation method and used as input three high frequency

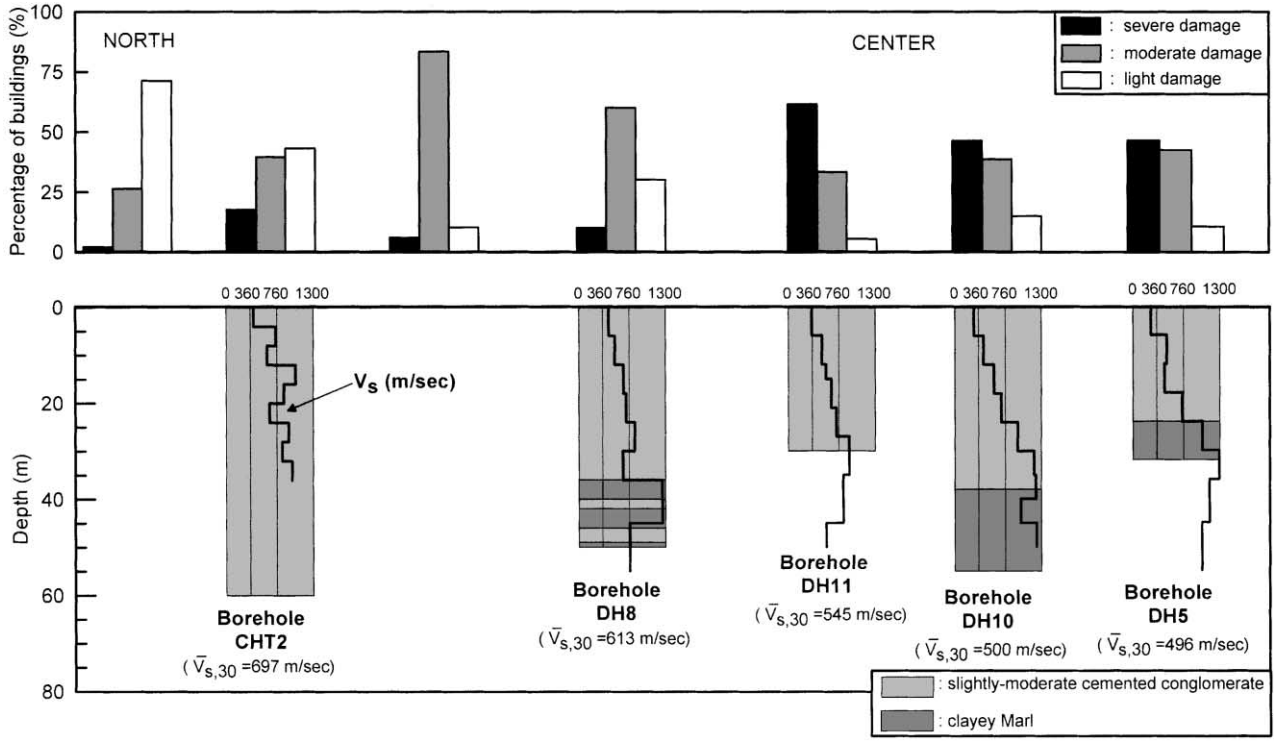

Fig. 12. Distribution of building damage and local soil conditions along a north–south section through Ano Liosia municipality.

Table 6
Statistical analysis of building properties in the northern and southern regions of Ano Liosia municipality

		Percentage of buildings	
		North—wider area of CHT2	Center—wider area of DH11, DH10 and DH5
Number of storeys	1	52	53
	2	40	37
	3	7	8
	>4	1	2
Date of construction	Before 1959	5	7
	Between 1959 ÷ 1985	62	71
	Between 1985 ÷ 1995	21	19
	After 1995	11	3
Type of load-bearing structure	Masonry	56	68
	Masonry and R/C	17	11
	R/C	19	7
	Other	8	14

excitations: two main shock simulations of the ground motion at rock-like formations within the epicenter area (FYL, PAR) ([36]), as well as, the main shock recording at the site of Dimokritos (DMK) scaled to the peak acceleration of the simulated motions, that is equal to 0.66 g. The significant period range of these excitations (0.09 ÷ 0.20 s) resembles closely that of the strong

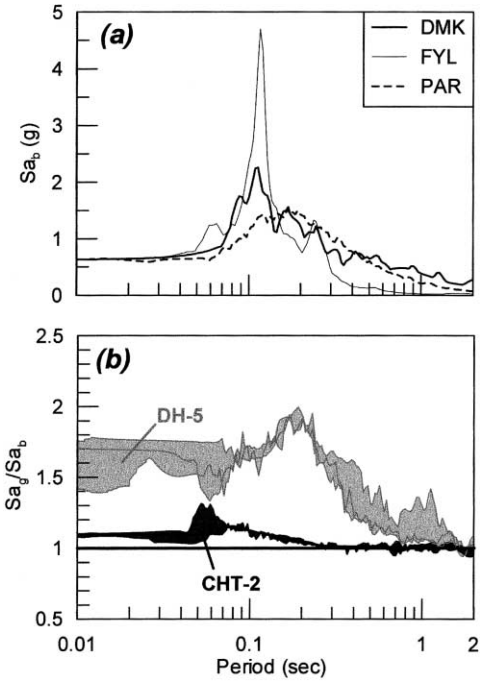

Fig. 13. (a) Elastic response spectra of high frequency input excitations and (b) spectral amplification ratio (ground surface over outcropping bedrock) predicted from the 1-D ground response analyses.

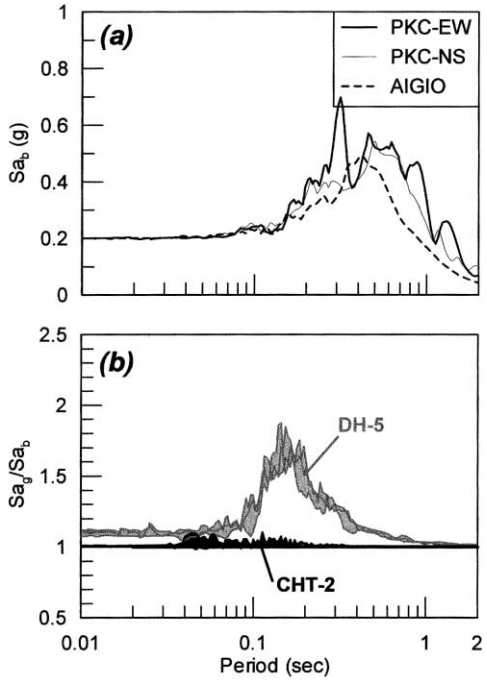

Fig. 14. (a) Elastic response spectra of low frequency input excitations and (b) spectral amplification ratio (ground surface over outcropping bedrock) predicted from the 1-D ground response analyses.

motion recordings obtained at Soft Rock sites, shown in Fig. 9(a).

The elastic response spectra of the input excitations are shown in Fig. 13(a), while the ratio of predicted ground motion-to-input excitation response spectra is shown in Fig. 13(b). It is evident that the two borehole sites exert entirely different effect on the seismic motion, despite their similarity in terms of geology and average shear wave velocity profiles. More specifically, for borehole DH5, soil amplification is significant in the period range of 0.00–0.40 s where most buildings of the area belong. On the contrary, soil amplification is negligible for borehole CHT2, which behaves essentially as seismic bedrock. The average predicted amplification of peak ground acceleration in borehole DH5 relative to borehole CHT2 is 46%, i.e. in fair agreement to the 40% amplification obtained from the analysis of strong motion recordings.

Comparing the fundamental period of the two borehole sites, 0.04 s for CHT2 and 0.18 for DH5, to the significant period range of the excitations (0.09 ÷ 0.20 s) it is realized that the observed amplification is probably a result of site-excitation resonance. To substantiate this view, the seismic ground response analyses were repeated for three lower frequency excitations, as shown in Fig. 14: two (PKC-EW and PKC-NS) from Northridge (1995) earthquake obtained at Pacoima Kangel Canyon station and one (AIGIO) from Aigio (1995) earthquake in southern Greece ([37]). The significant period range of these excitations is 0.27 ÷ 0.70 s, i.e. clearly higher than the fundamental period of both borehole sites. Observe that amplification is

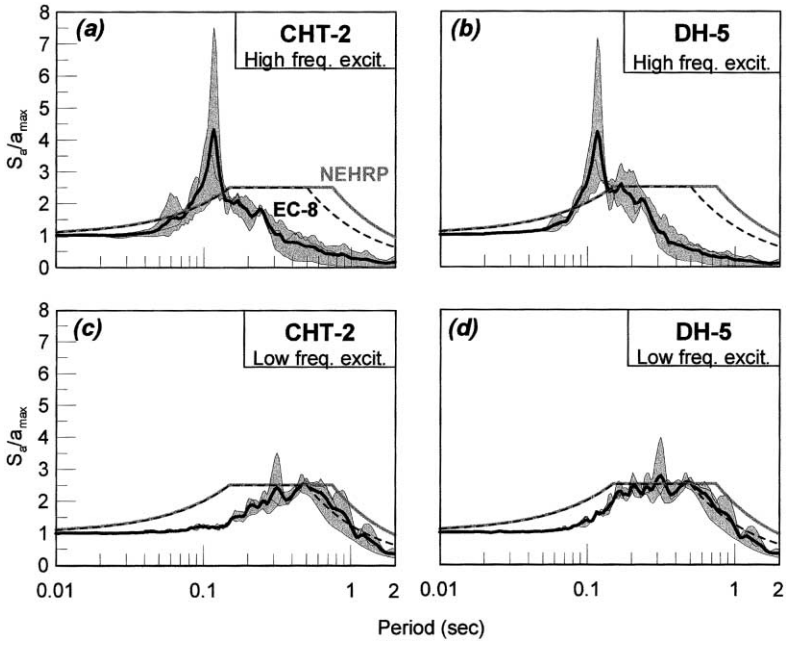

Fig. 15. Comparison between normalized elastic response spectra deduced from 1-D analyses, with the corresponding normalized design spectra proposed by NEHRP and EC-8.

now restricted to spectral accelerations in a narrow range around the fundamental period of borehole site DH5, not including the horizontal peak ground acceleration, while borehole site CHT2 behaves again as seismic bedrock.

The average elastic response spectra of the ground motion predicted for the high and the low frequency excitations are shown in Fig. 15(a) and (b), respectively. For purposes of comparison, these figures show also the design spectra of [1,2], drawn for site, acceleration and magnitude conditions similar to the analytical predictions. To focus upon site effects on the frequency content of the motions, all spectra have been normalized against the ground acceleration, i.e. the spectral acceleration at zero periods. As in the case of the strong motion recordings from the Athens Earthquake, site effects on the frequency content of predicted seismic ground motion are less significant compared to the effect on peak ground acceleration. Consequently, the unique spectrum provided by each code fits equally well the spectra predicted independently for the two borehole sites.

6. Summary and conclusions

The Athens earthquake ($Ms = 5.9$) of 7 September 1999 bears at least two characteristics commonly present in most recent destructive earthquakes. It was another example of rather moderate size seismic activity that causes destructive consequences due to its proximity to urban areas. In addition, it was certainly unexpected, in the sense that it originated from a previously unknown seismotectonic structure hidden among other well-established active faults.

From a geotechnical point of view, this earthquake will not be remembered for any spectacular ground failures (e.g. liquefaction, lateral spreading or landslides), as the two practically concurrent earthquakes of Kocaeli ($Ms = 7.4$) in Turkey and Chi-Chi ($Ms = 7.3$) in Taiwan. On the other hand, it provided a number of reliable strong motion recordings and well defined patterns of damage distribution at sites with known geological and geotechnical conditions. A joint evaluation of this evidence led to the following clues with regard the effect of the local ground conditions:

1. The *Stiff Soils* encountered within the Athens basin have amplified the peak ground acceleration relative to *Soft Rocks.* The average amplification deduced from the evaluation of strong motion recordings and the seismic ground response analyses performed at severely damaged areas, is 40 and 46%, respectively.
2. The effect of *Stiff Soils* on the frequency content of seismic ground motions, expressed through normalized elastic response spectra, is less significant and can be practically overlooked in the definition of seismic design actions.
3. From a theoretical point of view, the aforementioned phenomena are not surprising since the seismic excitation was rich in medium-to-high frequencies (3–15 Hz), which were selectively amplified by the Stiff Soil profiles. It is characteristic that seismic response analyses with a lower frequency input predicted similar response for *Stiff Soil* as well as for *Soft Rock* sites.
4. Despite the increase in the number of site (subsoil) classes, modern seismic codes [e.g. [1,2]] do not distinguish *Stiff Soils* from *Soft Rocks* and would not predict the local differentiation of seismic ground motion

Table A1
Definition of lithology (obtained from the geological investigations for Attico Metro SA)

UPPER DEPOSITS			
F:	Fill material		
AL (Alluvial deposits)			
AL1:	Silty clay to clayey silt (subrounded gravels)		
AL2:	Slightly to moderate cemented silty clay (gravel to pebble size subrounded particles)		
AL3:	Moderate to strongly cemented conglomerate		
AL4:	Poorly cemented conglomerate (sand to cobble particle size in a reddish clay matrix)		
Col/SD:	Colluvial deposits—slope deposits		
AL/Col:	Non differentiated alluvial colluvial deposits		
SUBSTRATUM			
Pliocene—Pleistocene deposits:			
Cg(M + L):	Conglomerate (limestone pebble to cobble size particles in a reddish silty clay matrix)		
"Athenian schist"—Sedimentary origin			
NDS:	Non differentiated schist	sh:	Shales
M:	Marl	s:	Siltstone
S:	Sandstone	s + L:	Calcareous siltstone
S + L:	Calcareous sandstone	G:	Grauwacke
B:	Breccia	BL or (B + L):	Limestone breccia
m:	Marlstone	L:	Limestone
Q:	Quartz	Ph:	Phyllite
"Athenian schist"—eruptive origin			
P:	Peridotite	D:	Diabase
Se:	Serpentine	Ps:	'Serpentinized' peridotite
BP:	Peridotite breccia	F:	Faulted zone

observed during the Athens earthquake. According to the evidence presented herein, this broad site (subsoil) class should be broken into two subclasses bearing the same design spectra but different, frequency dependent, site coefficients.

It is acknowledged that the field data presented earlier are not as bold as to dictate specific changes in seismic codes, before additional evidence from well documented case studies is collected and evaluated. Nevertheless, they shed light on a practical problem existent even in modern seismic codes and give preliminary guidelines for future improvement in code provisions.

Acknowledgements

The analysis of seismic recordings presented in the article is part of research sponsored by the Organization for Seismic Planning and Protection of Greece, the Technical Chamber of Greece and the National Technical University of Athens. The strong motion records were provided by the Geodynamic Institute of the National Observatory of Athens (NOAGI), the Institute of Engineering Seismology and Engineering Seismology (ITSAK) and the Public Power Corporation of Greece. In addition, Attiko Metro SA provided the geotechnical data for all subway stations where accelerographs were installed. In addition, the analysis of damages is part of a seismic microzonation study sponsored by Ano Liosia municipality. These contributions are deeply acknowledged.

Appendix A. Geological and geotechnical notation

The profile of Fig. 6 is presented in this article as a typical example of the geotechnical profiles established for the recording ([33]). It includes the geological description of the different layers, the standard penetration test results (N_{SPT}), the shear wave velocity (V_s), the plasticity index (I_P) and the mass density (ρ). The symbols used for the description of the various lithological units are explained in Table A1. In the presentation of the test data, different symbols are used in order to differentiate measurements obtained at different boreholes. In the presentation of SPT results, right arrows were used when a maximum number of blow counts was reached with penetration less than the 30 cm specified for termination of the test. In the same data, *R* denotes that no penetration was achieved during the test. The data regarding shear wave velocities have been deduced indirectly from N_{SPT}, according to the empirical relations proposed by [31] as described in the main text. In this case, the arrows denote lower limit values of V_s obtained from SPT results with partial or no penetration. The continuous black line denotes the

average velocity profile while the dashed black line the profile used to fit the fundamental site periods suggested by the seismological data.

References

[1] NEHRP (1997). Recommended provisions for seismic regulations for new buildings and other structures, Part 1: Provisions (FEMA 302).

[2] EC-8, 2000. Design provisions for earthquake resistance of structures, part 3: ground conditions and seismic action. prEN 1998-1, Draft May 2000, European Committee for Standardization, Brussels.

[3] US Geol. Surv. (USGS) National Earthquake Information Center, World Data Center A for Seismology, http://wwwneic.cr.usgs.gov/neis/FM/Q99090711156.html

[4] Harvard CMT catalog, http://www.seismology.harvard.edu.

[5] University of Thessaloniki, Geophysical Laboratory (GLUT), http://lemnos.geo.auth.gr/.

[6] Stavrakakis GN, Chouliaras G, Panopoulou G. Seismic source Parameters for the $M_L = 5.4$ Athens Earthquake (September 7, 1999) from a New Telemetric Broad band Seismological network in Greece. Natural Hazards, Special Volume on the Athens Earthquake (in press).

[7] Papadopoulos GA, Drakatos G, Papanastasiou D, et al. Preliminary results about the catastrophic earthquake of 7 September 1999 in Athens, Greece. Seismological Research Letters 2000; 71(3): 318–29.

[8] Voulgaris N, Kassaras I, Papadimitriou P, Delibasis N. Preliminary results of the Athens September 7, 1999 aftershock sequence, Annales Geologiques des Pays Helleniques, 1e serie, T. XXXVIII, Fasc. B.

[9] Tselentis GA, Zaradnik Z. The Athens Earthquake of 7 September 1999, BSSA 2000; 90(5): 1143–60.

[10] National Observatory of Athens, Geodynamic Institute (NOAGI), http://gein.noa.gr.

[11] Voulgaris N, 2001. Personal Communication.

[12] Tselentis GA, Zaradnik Z. Aftershock monitoring of the Athens earthquake of 7 September 1999. Seismological Research Letters 2000a; 71(3): 330–7.

[13] Sargeant SL, Burton PW, Douglas A, Evans JR. A source model for the 7th September 1999 Athens earthquake. Proc. XXVII General Assembly of the European Seismological Commission, September, 2001. p. 138–42.

[14] Kontoes C, Elias P, Sykioti O, Briole P, et al. Displacement field and fault model for the September 7, 1999 Athens earthquake inferred from ERS2 satellite radar interferometry. Geophysical Research Letters 2000;27(24):3989–92.

[15] Pavlides S, Papadopoulos GA, Ganas A. The 7th September unexpected earthquake of Athens: preliminary results on the seismotectonic environment. 1st Conf. Advances in Natural Hazards Mitigation: Experiences from Europe and Japan, Athens 3–4 November, 1999. p. 80–5.

[16] Pavlides S, Papadopoulos GA, Ganas A. Seismic hazard in urban areas: the 7th September 1999 Athens earthquake case study. In: Okumura K, Takada K, Goto H, editors. Proceedings of the Hokudan International Symposium and School on Active Faulting: Active Fault Research for the New Millenium, January 17–26, 2000.

[17] Ambraseys N. Material for the investigation of the seismicity of Central Greece. In: Albini P, Moroni A, editors. Historical Investigation of the Seismicity of European Earthquakes, vol. 2. 1994. p. 1–10.

[18] Rodoyanni, T., Mettos, A., Galanakis, D., Georgiou, C., 2000. The Athens earthquake of September 7, 1999: its setting and effects, Annales Geologiques des Pays Helleniques, 1e Serie, T. XXXVIII, Fasc. B.

[19] Elnashai AS, Ambraseys NN. Observations of two recent earthquakes Kocaeli, Turkey and Mt Parnes, Greece. In: Elnashai AS, Antoniou S, editors. Implications of Recent Earthquakes on Seismic Risk, Textbook, Imperial College Press, 2000.

[20] Nakamura Y, 1989. A method for dynamic characteristics estimation of subsurface using microtremors on the ground surface. RTRI, Quarterly Report 30 (1), Japan.

[21] Theodoulidis N, Archuleta RJ, Bard PY, Bouchon M, 1996. Horizontal-to-vertical spectral ratio and geological conditions: the case of Garner Valley Downhole array in Southern California. BSSA, p. 1692–1703.

[22] Bonilla FL, Steidl JH, Lindley GT, Tumarkin AG, Archuleta RJ, 1997. Site amplification in the San Fernando Valley, CA: variability of site effect estimation using the S-wave, Coda and H/V methods. BSSA, vol. 87, p. 710–30.

[23] Yamazaki F, Ansary MA. On the stability of horizontal-to-vertical spectral ratio of earthquake ground motion. Bull. ERS 1997;30:27–44.

[24] Dimitriou P, Kalogeras I, Theodoulidis N. Evidence of nonlinear site response in horizontal-to-vertical spectral ratio from near-field earthquakes. Soil Dynamics and Earthquake Engineering 1999;18:423–35.

[25] Trifunac MD, Todorovska MI. Can aftershock studies predict site amplification factors? Northridge, CA, earthquake of 17 January 1994. Soil Dynamics and Earthquake Engineering 2000;19:233–51.

[26] Trifunac MD, Todorovska MI. Long period microtremors, microseisms and earthquake damage: Northridge, CA, earthquake of 17 January 1994. Soil Dynamics and Earthquake Engineering 2000;19:253–67.

[27] Joyner WB, Furnal TE, Glassmoyer G, 1994. Empirical spectral response issues from an eastern US perspective. In: Martin GR, editor. Proceedings of the 1992 NCEER/SEAOC/BSSC Workshop on Site Response During Earthquakes and Seismic Code Provisions. University of Southern California, Los Angeles, November 18–20, 1992, National Center for Earthquake Engineering Research Special Publication NCEER-94-SP01, Buffalo, NY.

[28] Mucciarelli M, Bettinali F, Zaninetti M, Vanini M, Mendez A, Galli P. Refining Nakamura's technique: processing techniques and innovative instrumentation. Proceedings of ESC Assembly, Reykjavik, September, 1996. p. 411–6.

[29] Dobry R, Idriss IM, Power MS. New site coefficients and site classification system used in recent building seismic code provisions. Earthquake Spectra 2000;16(1):41–67.

[30] Schnabel P, Lysmer J, Seed HB, 1972. SHAKE: a computer program for conducting equivalent linear seismic response analysis of horizontally layered soil deposits. University of California in Berkeley, Earthq. Engineering. Research Center, Report No. UCB/EERC 72/12.

[31] Imai T, Tonuchi K, 1982. Correlation of N_{SPT} value with S-wave velocity and shear modulus. Proceedings of the second European Symposium on Penetration Testing, Amsterdam, May 24–27.

[32] Vucetic M, Dobry R. Effect of soil plasticity on cyclic response. Journal of Geotechnical Engineering, ASCE 1991;117(1):89–107.

[33] Bouckovalas GD, Kouretzis G, Kalogeras Y, 2001. Site-specific analysis of strong motion data from the September 7 1999 Athens, Greece earthquake. Natural Hazards, Special Volume on Athens Earthquake (in press).

[34] Abrahamson NA, Silva W, 1997. Empirical response spectral attenuation relations for shallow crustal earthquakes. Seismological Research Letters 68 (1).

[35] Bouckovalas GD, Papadimitriou A, Kouretzis G, et al. 2000. Seismic microzonation of Ano Liosia municipality: evaluation of site effects. Technical Report, National Techn. Univ. of Athens, Dept. of Civil Engineering, Soil Dynamics Laboratory.

[36] Makropoulos K, 2000. Seismic hazard assessment in the area of Ano Liosia municipality, Technical Report, Athens University, Dept. of Geophysics and Geothermal, Seismological Laboratory.

[37] Bouckovalas G, Gazetas G, Papadimitriou A, 1999. Geotechnical aspects of the Aegion (Greece) earthquake. Proceedings of 2nd International Conference on Geotech. Earthq. Engineering, Lisbon, June.

Further reading

More general information about the Athens Earthquake can be found in the following bibliography and relevant websites.

[1] Athanasopoulos GA, Pelekis PC, Xenaki VC, 2001. Topography effects in the Athens 1999 Earthquake: the case of Hotel Dekelia. Proceedings of the 4th International Conference on Recent Advances in Geotechnical Earthquake Engineering and Soil Dynamics, San Diego CA, March 28–31 (CD-ROM I).

[2] Kallou PV, Gazetas G, Psarropoulos PN, 2001. Topography and soil effects in the $Ms = 5.9$ Athens Earthquake: the case of Adames. Natural Hazards Special Volume on the Athens Earthquake (in press).

[3] Marinos P, Bouckovalas GD, Tsiambaos G, Sabatakakis N, Antoniou A. Ground zoning against seismic hazard in Athens, Greece. Int. Journal of Engineering Geology 2001 (in press).

[4] Papadimitriou P, Kaviris G, Voulgaris N, Kassaras I, Delibasis N, Makropoulos K, 2000. The September 7, 1999 Athens Earthquake Sequence recorded by the CORNET Network: Preliminary Results of Source Parameter Determination of the Mainshock, Annales Geologiques des Pays Helleniques, 1e Serie, T. XXXVIII, Fasc. B.

[5] Pavlides S, Papadopoulos GA, Ganas A, 2001. The fault that caused the Athens September 1999, Ms = 5.9 Earthquake: field observations. Natural Hazards, Special Volume on the Athens Earthquake (in press).

[6] Pomonis A. The Athens Earthquake: a disaster management perspective. Natural Hazards, Special Volume on Athens Earthquake 2001 (in press).

[7] Psycharis I, et al. 1999. The Athens, Greece Earthquake of September 7, 1999. EERI Special Earthquake Report.

[8] Sargeant SL, Burton PW, Douglas A, Evans JR. [2000]. Teleseismic body waveform modelling of the Athens Earthquake, September 7, 1999. Natural Hazards, Special Volume on the Athens Earthquake (in press).

[9] Institute of Engineering Seismology and Earthquake Engineering http://www.itsak.gr/.

[10] Department of Geophysics-Geothermics, Faculty of Geology, Athens University http://www.geophysics.geol.uoa.gr/.